Magnetic Resonance Imaging 62 (2019) 191–198

Contents lists available at ScienceDirect

Magnetic Resonance Imaging

journal homepage: www.elsevier.com/locate/mri

Original contribution

A "flared-end" gradient coil with outer-wall direct cooling for human brain imaging: A feasibility study

Zhi Yang[a], Beihan Zhao[a], Yong Pei[a], Bao Yang[a,*], Hanbing Lu[b,*]

[a] Department of Mechanical Engineering, University of Maryland, College Park, MD 20742, USA
[b] Neuroimaging Research Branch, National Institute on Drug Abuse, National Institutes of Health, Baltimore, MD 21224, USA

ARTICLE INFO

Keywords:
Gradient insert
Local gradient coil
Head-only MRI
Cooling

ABSTRACT

Optimal gradient performance is arguably a pre-requisite to realize the full potential of ultrahigh field magnetic resonance imaging (MRI). The values of using tailored gradient coils for brain imaging have been well acknowledged. Unfortunately, conventional head-only gradient coils have two major technical limitations, i.e. limited shoulder clearance and limited cooling capacity. A design, coined "flared-end" gradient coil, combined with a cooling method, named "outer-wall direct cooling", is proposed to address these problems. The "flared-end" design permits brain access to the center of gradient coil. The "flared end" structure is 3D-printed. It has electrical winding patterns (grooves) on one side and evenly spaced cooling channels on the opposite side. Electrical conductor (copper wire) is fixed into the grooves; coolant is in direct contact with the outer surface of the electrical conductor above each cooling channel, eliminating interfacial thermal resistance between coolant and copper wires. Heat transfer area is thus determined by the size and the number of cooling channels. This approach allows high electric current density for high gradient field strength while maintaining high cooling efficiency. Additionally, the symmetric coil geometry guarantees intrinsic torque balance. As a proof of concept, we have made a gradient coil prototype without active shielding. This coil has an inner diameter of 0.3 m, and is capable of generating 0.337, 0.225 and 0.485 mT/m/A along X, Y and Z, respectively. Active shielding was designed theoretically, but not pursued in the construction of this coil prototype. The new coil geometry and cooling method offer a novel avenue for new gradient coils tailored for human brain imaging at ultrahigh field.

1. Introduction

The performance of the gradient coil is one of the primary limiting factors in high speed, high resolution magnetic resonance imaging (MRI), and in diffusion MRI [1]. Conventional MRI scanners are designed to cover a large field of view. The gradient strength and the inductance of these coils are thus inherently limited by the physical size of the coil [2,3]. Increasing electrical current and voltage outputs of a gradient amplifier has been the major technical pursuit to enhance gradient performance. The "connectome gradient coil" is an exemplar along this line [4]. However, as electrical current (I) increases, ohmic heating (Q) also becomes more pronounced, because $Q \propto I^2$. As a result, efficient coil cooling to dissipate the heat becomes critical. Furthermore, out of safety considerations, peripheral nerve stimulation (PNS) and cardiac stimulation (CS) are two physiological factors that ultimately limit the performance of a gradient coil. PNS and CS thresholds are related to $d\boldsymbol{B}/dt$. Here $\boldsymbol{B}$, the magnetic field strength, can be expressed as $\int \boldsymbol{G}(r)dr$, $\boldsymbol{G}$ is the gradient field along r. For a body gradient coil, $\boldsymbol{G}$ typically extends to a large distance, and thus possesses a high risk to induce PNS and CS [5,6]. It would thus appear suboptimal to employ a whole-body gradient coil to image the brain.

The pioneering development of local gradient insert enabled fast imaging sequence such as echo planar imaging [7,8] and high resolution MRI to be implemented on clinical scanners [9,10], and helped open the era of functional MRI [11,12]. Nevertheless, there are two major technical problems associated with conventional gradient insert design: 1) "shoulder clearance": in conventional cylindrical coil design, the coil has to reach certain length in order to achieve a volume with high fidelity to the linear gradient field suitable for human brain imaging. However, because the inner diameter of the cylindrical coil typically does not clear the shoulders of a typical adult, it is quite unfortunate that, quite often, one can't place the center of the human brain to the center of the gradient coil (see Fig. 1A for illustration). In many cases, only half of the "sweet spot" is used for neuroimaging. 2) cooling: modern gradient amplifiers capable of providing 600 A or more current are readily available. Such high current generates tremendous

* Corresponding authors at: 251 Bayview Blvd, Suite 200, Rm7A727, Baltimore, MD 21224, USA.
E-mail addresses: baoyang@umd.edu (B. Yang), luha@mail.nih.gov (H. Lu).

https://doi.org/10.1016/j.mri.2019.07.006
Received 28 April 2019; Received in revised form 11 July 2019; Accepted 11 July 2019
0730-725X/ Published by Elsevier Inc.

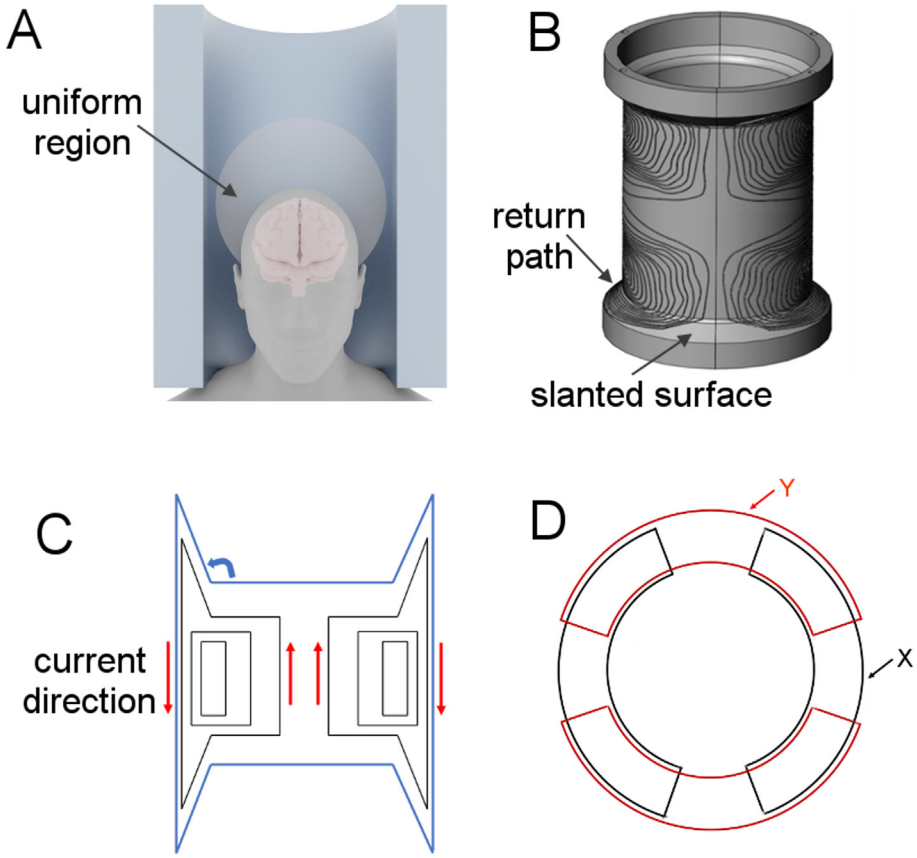

Fig. 1. A. Illustration of the "shoulder clearance" problem in conventional head-only gradient coil. The shoulder cannot fit into a typical head-only gradient coil; only part of the uniform region is used for imaging a typical human brain. **B** and **C**, "flared-end" coil design. By placing the return paths on the slanted surface parallel to the shoulder, one can shorten the overall length of the coil, and thus minimizing the "shoulder clearance" problem. X and Y gradients have similar winding patterns, but shifted by 90°. **D**, front view of the "flared end" coil.

amount of heat [13]. For example, assuming a resistance of 0.5 Ω, with an electrical current of 600 A and 60% duty cycle, the ohmic heating would be 108 kW from a single gradient coil. Driving three gradient coils simultaneously (as in diffusion imaging) would triple the amount of heating. The small size of a head-only gradient coil exacerbates the heating problem due to reduced coil mass and volume available for cooling tubes.

To mitigate the "shoulder clearance" problem, many previous approaches have relied on asymmetric head gradient designs [14–19]. These designs are appealing because i) it reduces the potential of PNS and CS since the shoulders and torso are outside of the main gradient field; ii) the linear volume is at the end of the cylinder, and thus eliminates the "shoulder clearance" problem. However, as discussed by Setsompop et al. [4], the asymmetric head gradient also has several undesirable features: i) the design is harder to balance the torque and to provide effective eddy current shielding; ii) the linearity of the gradient field is much poorer than conventional symmetric design; iii) the Maxwell terms (concomitant terms) include odd orders as well as even orders, complicating their effect on the diffusion pulse sequence [20]. While some of these problems, such as image distortions associated with gradient field nonlinearity might be manageable by reconstruction processing [21,22]; in diffusion MRI, b-factors associated with diffusion concomitant terms and their effect on fiber tracking might be less straightforward to quantify.

"Folded gradient" design is another approach to mitigate the "shoulder clearance" problem [23,24]. In a conventional cylindrical transverse gradient coil design, the segments in the middle of coil (active segments) contribute to the desired magnetic field, while the segments on both ends of the coil (return paths) generate undesirable field and contribute to the overall length of the coil. One can fold the return paths toward the center of the coil, thus shortening the length of the coil. A limitation of this design is that the gradient field is highly non-linear, because the active segments and an equal number of return paths are both placed toward the center of the coil, and the magnetic fields generated by them have opposite signs; it is a challenge to optimize the magnetic field in the target volume due to physical constraints. Notably, a conceptually similar, but more extreme approach had been reported by Mansfield and others [25,26]: the return paths were co-axial to the active segments along the radial direction, and thus did not contribute to the overall length of the coil; a further optimization of gradient field based on co-axial return paths called "sandwich" gradient coil design, was previously proposed by Lu et al. [27]. In this approach, wire loops are embedded in circular planar disks. The active segments of each loop are placed close to the internal surface and the return paths are placed close to the outer surface of the disk. The disks are then sandwiched together. Active segments surrounding the internal surface generate the desired field, while the return paths serve as shielding. The advantage of "sandwich" gradient coil is that it can be very short, and thus eliminates the "shoulder clearance" problem, and the gradient field can be highly uniform; one limitation is that the efficiency is relatively lower than conventional transverse gradient coil.

Anatomically, the outlines of neck and shoulder have an angle of about 115° (Fig. 1A). One can take advantage of this feature and design a slanted surface that is parallel to the shoulder outline and place the return paths on the slanted surface (see Fig. 1B–C). With both ends flaring out, the return paths are no longer a limiting factor that prevents the brain from reaching the "sweet spot" of the coil. The X and Y gradients have similar wiring patterns but shifted by 90°. Fig. 1D illustrates the view from either end. Furthermore, with modern high-power gradient amplifiers, efficient dissipation of ohmic heat becomes a technical challenge, which is particularly critical for head-size gradient coils due to limited room for cooling tubes. We present a novel approach, called "outer-wall direct cooling", for effective heat dissipation. As a proof-of-concept, we have built a prototype gradient coil.

2. Methods

2.1. Gradient field optimization

The proposed coil does not have a classical cylindrical or planar geometry, and thus lacks an analytical solution [3]. Non-linear optimization approach, such as the momentum-weighted conjugate gradient decent (CGD) method described by Lu et al. [27], is suitable for designing the winding patterns.

The size of a head-only coil is much smaller than a whole body gradient coil, the inductance is thus not a major concern; Furthermore, given the symmetry in coil geometry, the torque is intrinsically balanced, and the net force is zero assuming uniform B_0 (see discussion for nonuniform B_0), we thus focused on gradient field strength and field fidelity, and defined the cost function as:

$$E = \sum_{m=1}^{M} (B_m - \overline{B}_m)^2 \tag{1}$$

Here $\overline{B}_m$ is the desired magnetic field at the mth point in the region of interest (ROI, or the target field), B_m is the calculated magnetic field at the same point, and M is the total number of points prescribed in the ROI. It is apparent that E is a function of the coordinates of the wire elements. The goal is to find the optimum coordinates for each of the wire elements $p_0, p_1, p_2, \ldots, p_N$, such that the cost function E is minimal.

The following constraints were applied to ensure that the design be practical for construction: (i) current must be continuous; (ii) the space between neighboring wires should be greater than defined minimum values; (iii) the wire elements should be within defined physical dimensions of the coil; and (iv) there must be no crossover between wires. These constraints can be readily satisfied when the variable to be optimized is one-dimensional. For example, for a Z gradient coil on a cylindrical surface, the variables to be optimized are the z coordinates of the wire loops of constant diameters (in cylindrical coordinates (r, φ, z)). For the X and Y gradients shown in Fig. 1, all three coordinates (r, φ and z) need to be optimized. Specifically,

$$\begin{bmatrix} r_{0,i+1} & \varphi_{0,i+1} & z_{0,i+1} \\ r_{1,i+1} & \varphi_{1,i+1} & z_{1,i+1} \\ \cdots & & \\ r_{N,i+1} & \varphi_{N,i+1} & z_{N,i+1} \end{bmatrix} = \begin{bmatrix} r_{0,i} & \varphi_{0,i} & z_{0,i} \\ r_{1,i} & \varphi_{1,i} & z_{1,i} \\ \cdots & & \\ r_{N,i} & \varphi_{N,i} & z_{N,i} \end{bmatrix} + \alpha_i \cdot \begin{bmatrix} dr_{0,i} & d\varphi_{0,i} & dz_{0,i} \\ dr_{1,i} & d\varphi_{1,i} & dz_{1,i} \\ \cdots & & \\ dr_{N,i} & d\varphi_{N,i} & dz_{N,i} \end{bmatrix} \cdot \begin{bmatrix} \beta & 0 & 0 \\ 0 & \gamma & 0 \\ 0 & 0 & 1 \end{bmatrix} \tag{2}$$

Here $dr_{m,\,i}$, $d\varphi_{m,\,i}$, $dz_{m,\,i}$ are the search directions of the mth wire segment, at the ith iteration, along r, φ and z, derived from the conjugate gradient descent algorithm [9]; α_i is the step size along z at the ith iteration, β and γ are defined according to the following 2 conditions:

(i) for Z gradient coil design, $\beta = \gamma = 0$.

(ii) for X/Y gradient coil design, β and γ are the momentum weightings of the step sizes for the radial and azimuthal coordinates. α, β and γ are determined based on the first order partial derivatives of E over r, φ and z (i.e. $\partial E/\partial r$, $\partial E/\partial \varphi$, $\partial E/\partial z$), and are detailed in reference (27). We start with an empirical desired gradient field strength G_i, define the corresponding $\overline{B}_m$, and find the spatial distribution of the wire elements $p_0, p_1, p_2, \ldots, p_N$, such that the cost function E is minimal. We then increase or decrease G_i by 3 mT/m, depending on the optimization results, and repeat the above non-linear optimization procedures. The optimal design is reached after 20–30 iterations. The initial positions of the wire elements $p_0, p_1, p_2, \ldots, p_N$ were prescribed mathematically, and was somewhat arbitrary. However, after 2–3 trials, an initial pattern could be readily prescribed. In our experience, the final pattern did not depend strongly on the initial pattern, since a "bad" initial pattern could be corrected during the optimization stages that followed.

2.2. Cooling design

As stated above, with modern high-power gradient amplifiers, ohmic heating is a serious concern in gradient coil technology. Conventional gradient coil thermal management can be classified into 3 categories: i) natural convection on the external surface of gradient coil assembly; ii) forced convection between the coolant inside a tube and adjacent current-carrying element with insulation dielectric material in between (here we call it "indirect cooling" for convenience); and iii) forced convection with the coolant inside the current-carrying element (e.g. copper tube) of the gradient coil assembly (called "internal direct cooling"). Natural convection suffers from extremely low heat transfer coefficient, leading to limited cooling capacity, thus is not discussed here. The physics of heat transfer related to "direct cooling" method is detailed in Appendix A.

It follows from Eq. (A-1) in Appendix A that better cooling performance can be achieved by two approaches: i) enhancing heat transfer coefficient h; and ii) maximizing heat transfer area A. The materials, such as high thermal conducting epoxy, used to stabilize electric current carrying materials (e.g. copper wires), typically have a thermal conductivity (h) of < 2.5 W/mK. In contrast, copper has a thermal conductivity of about 380 W/mK. It thus appears that direct cooling inside copper tubing (i.e. "internal direct cooling") is a preferred approach by eliminating insulating materials between coolant and copper tubing. However, high pressure drop ΔP associated with internal cooling approaching must be taken into accounts as well.

For internal direct cooling, the size of the copper tubing is a delicate tradeoff between cooling efficiency and gradient field efficiency. A large tubing diameter (D) leads to a large heat transfer area A, and is thus preferred for thermal transfer. However, a small diameter leads to high electric current density, and thus preferable to achieve high gradient field strength per unit current. Furthermore, pressure drop ΔP is associated with flow rate (a key factor in determining cooling efficiency) and copper tubing dimensions, and needs to be evaluated (see Eq. (A-9) in Appendix A) to achieve required cooling efficiency (see Eqs. (A-2) to (A-8) in Appendix A). Fig. 2 illustrates theoretical simulations of thermal performance and pressure drop with the internal direct cooling approach. The analytical calculation was performed with a copper tubing with 1.6 mm and 3.2 mm as inner and outer diameter, respectively. The overall length was 15 m. When the copper tubing carries 200 Amp current, massive ohmic heating will be generated inside copper tubing (Eq. (A-8)) therefore, high flow rate of dielectric coolant Duratherm 450 Oil will be vital to achieve desired thermal performance. As mentioned earlier, flow rate is a trade-off between thermal performance and pressure drop. Thus, the flow rate was systematically adjusted to identify the optimal point for both acceptable thermal performance and pressure drop. As shown in Fig. 2, the nature of coolant flow transits from laminar to turbulent flow at ~0.75 l per minute (LPM), where effective heat transfer coefficient is improved dramatically. As a result, the sharp enhancement in heat transfer coefficient of coolant, copper tube surface temperature at the outlet decreases dramatically at 0.75 LPM. The transition phase between laminar and turbulent flow regime provides moderate increment in heat transfer coefficient from laminar flow. However, the pressure drop across the copper tube is proportional to square of coolant velocity. In such case, it is extremely challenging to maintain low surface temperature using high flow rate while keep the pressure drop in a reasonable range (< 1500 kPa), because practically most materials (e.g. hoses and tubes) cannot stand high pressure. As such breaking the tube into short segments is necessary, which complicates the cooling design.

2.3. Alternative approach: outer-wall direct cooling

To resolve the dilemma associated with internal-wall direct cooling

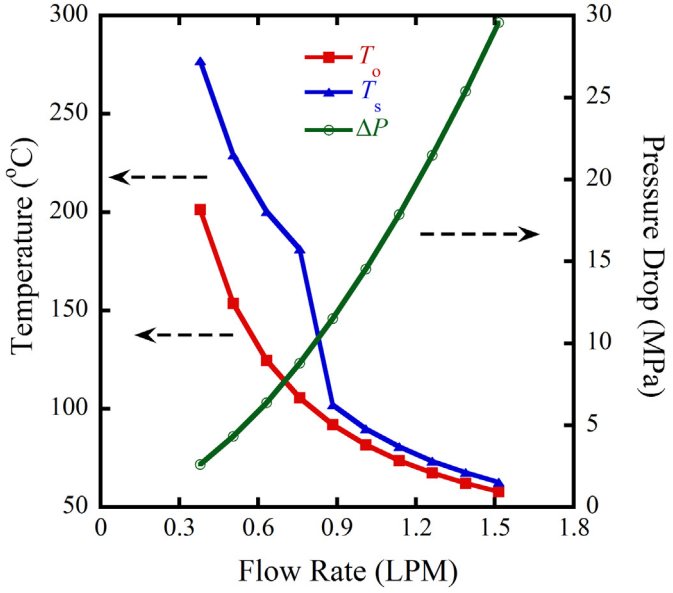

Fig. 2. Theoretical simulation of temperature and pressure drop across a copper tube as a function of flow rate. Simulation parameters: copper tube length = 15 m, ID = 1.6 mm, OD = 3.2 mm, current 200 A, coolant: Duratherm 450 Oil. Note that very high pressure drop across the copper tube (> 27 MPa) is necessary to achieve a temperature of 60 °C. Red curve (T_o): coolant outlet temperature; blue curve (T_s): copper tubing surface temperature at coolant outlet; green curve (ΔP), pressure drop across the copper tube. (For interpretation of the references to colour in this figure legend, the reader is referred to the web version of this article.)

described above, we propose a novel method. Fig. 3 illustrates our design approach. Instead of using copper tubes as the electrical conductor which demands tremendous pressure and pump power to circulate coolant inside, solid electrical conductors (e.g. copper wires) are proposed with coolant in direct contact with the outer surface of the conductor. Specifically, we 3D-print a frame that has electrical winding patterns (grooves) on one side and cooling channels on the opposite side. A total of 36 cooling channels, each 17.2 mm in width, 4.7 mm in depth, are evenly distributed along the frame. The electrical conductor (copper wire) is fixated into the grooves using epoxy; coolant flows inside the cooling channels, in direct contact with one side of the electrical conductor above the cooling channels, eliminating interfacial thermal resistance. The number of cooling channels and coolant distribution were determined based on theoretical thermal modeling. This method relaxes system pressure and pump power requirements while still benefits from direct cooling. This approach is referred as "Outer wall direct cooling."

3. Results

3.1. Coil design

We have applied the above non-linear optimization method to design a three-axis torque-balanced gradient coil for human brain imaging. The inner-most layer was Z with a conventional cylindrical shape, followed by X and Y, which have cylindrical shape in the middle and slanted surfaces at both ends. The length of Z cylinder is 28 cm, which is the effective length of the coil. The inner diameter of Z is 30 cm, identical to the one by Wong et al. [28] for human brain imaging. The outer most diameter in the slanted surface is 46.5 cm. This diameter was chosen to ensure enough clearance so that the coil could be placed on the patient tables of the commercial MRI scanners, and could be conveniently moved into/out of the magnet without the need for additional mounting structure. The angle between the cylindrical surface and the slanted surface is 115°.

The Z coil has a total of 38 loops of wires; the X and Y gradients have 18 and 13 loops of wires in each quadrant, respectively. Part of the return paths in X/Y coils rest on the cylindrical surface; the remaining return paths are embedded on the slanted surfaces (see Fig. 3A). Each loop is divided into 128 wire segments. For the X/Y gradient, each wire segment has 3 variables (x, y and z) to be optimized; for the Z gradient, only the z coordinates need to be optimized. A sphere of 21 cm at the center of the coil is defined as the region of interest (ROI) to be optimized. Due to intrinsic symmetry of the field distribution, 90 points in one octant of the sphere is defined as the discrete ROI for X/Y optimization; 45 points in one rectangular plane ($x = 0$, $y \geq 0$) for Z. The desired magnetic field at each point ($\overline{B_m}$) is defined. The magnetic field at each point of the ROI (Bm) is calculated. The goal is to optimize the coordinates of these wire segments so that the cost function is minimal under the physical constraints. The optimization code was written in standard C language on a personal computer running Linux. The optimization process was performed iteratively. Table 1 lists coil specifications.

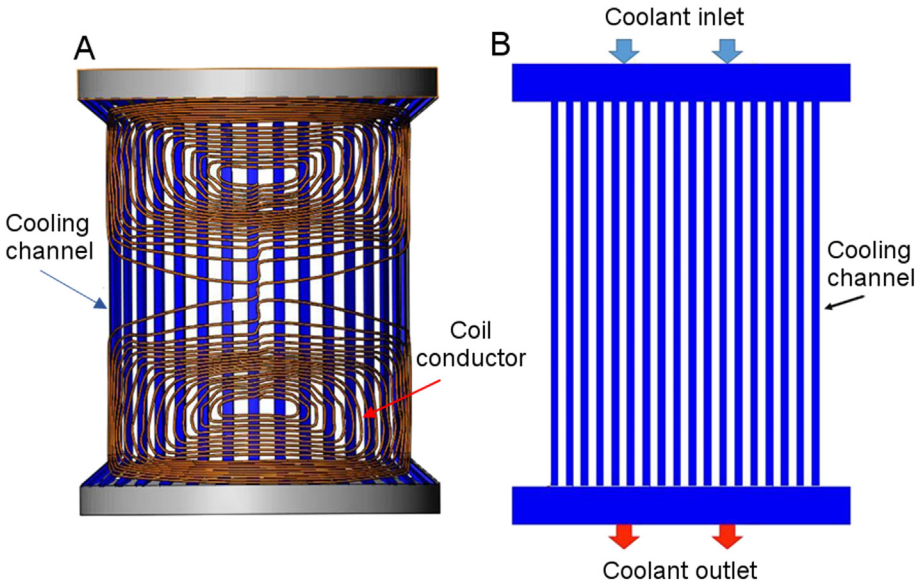

Fig. 3. Schematic of "outer-wall direct cooliSV0049ng" for an "flared-end" gradient coil. **A**: Wiring patterns for a transverse gradient (X/Y) are shown in brown. The return paths of the coil electrical conductors are placed on a slanted surface to mitigate the "shoulder clearance" problem. Coolant flows inside cooling channels in direct contact with the electrical conductors, eliminating interfacial thermal resistance between coolant and copper wires. Heat transfer area is determined by the size and the number of cooling channels, not by the inner diameter of a copper tube. This approach allows high electric current density for high gradient field strength while maintaining high cooling efficiency. Coolant inlet and outlet are optimized for thermal performance and pressure drop (**B**). (For interpretation of the references to colour in this figure legend, the reader is referred to the web version of this article.)

Table 1
Coil specifications.

Gradient axis	# of wire loops	Field fidelity (RMS)		Gradient field mT/m/A current	Inductance (μH)	Resistance (ohm)
		21 cm dia. sphere[a]	17 cm dia. sphere[a]			
X	18 × 4	8.94%	2.69%	0.337	228	0.49
Y	13 × 4	10.62%	3.36%	0.225	152	0.44
Z	19 × 2	4.83%	2.31%	0.485	126	0.24

[a] Calculated within a band of 14 cm in the middle of the sphere with a diameter of 17 or 21 cm. Inductance and resistance are readings from measurements. Gradient field parameters are calculated from designed winding patterns.

3.2. Coil construction

Given the unique shape of coil windings and cooling design for X/Y gradients, it is a challenge to build a porotype with conventional machining technologies. We applied the additive 3D printing techniques to build major frames for X and Y gradients with designed shape, winding patterns and cooling channels. The X/Y gradient was divided into 4 quadrants/modules. Each module was printed individually before final assembly. Z gradient was constructed with G10 fiberglass using 4 axis CNC machine due to its relatively simple geometry. Solid copper wires (Gauge 12) were embedded into individual X, Y and Z gradients. The three gradients were potted together with high thermal conductivity and high dielectric strength epoxy. Worth of mention, while most 3D printing materials are weak in nature, and cannot stand the mechanical stress that the current-carrying elements would experience inside a magnet, some 3D printing materials, combined with low-viscosity epoxy produce fiberglass-like structures, and can stand very high mechanical stress (see discussion for more details).

3.3. Cooling test and magnetic field mapping

To measure the cooling effect and to compare cooling efficiency between direct and indirect (forced convection) cooling, Z gradient was designed to have no cooling channels. It is cooled by coolants flowing inside the cooling channels in X and Y. Temperature sensors (K type thermocouple, Gauge 40) were embedded inside epoxy uniformly to monitor cooling performance in X, Y and Z gradients. Magnetic field was measured with a Gaussmeter (Model MR3, Alphalab Inc., Salt Lake City, Utah, USA). A 7 × 9 grid frame was 3D-printed to allow for consistent positioning of the magnetic field probe inside the coil. The grids cover an area of 49.5 × 24.1 cm^2. Fig. 4 shows the prototype gradient coil with cooling system. Fig. 5 illustrates magnetic field distribution for X, Y and Z coils. The spatial distribution of the linearity and homogeneity of the gradient field are generally consistent with theoretical calculations shown in Table 1.

3.4. Cooling measurement

Table 2 lists temperature readings for X gradient (readings from Y were similar to X and are not presented). The measurement was performed with a constant voltage DC power supply capable of a maximum of 21 V output. DC current = 42.1 A (maximum in our experimental setting for X gradient testing), coolant flow rate = 20.14 LPM for the entire active gradient layer. An increase in coolant outlet temperature by 1.3°C indicates overall effective heat removal capability with the outer-wall direct cooling approach. Further improvement in cooling can be expected by increasing the coolant flow rate.

Table 3 lists temperature readings for Z gradient. As stated above, there was no direct-cooling for Z. Instead, the coolant was directed to X gradient to provide any possible cooling for Z gradient through potting epoxy and 3D printed part of X gradient. Constant voltage DC power supply was set to 19.2 V, and current was 80 A, coolant flow rate = 20.14 LPM. As expected, heat propagated mainly from Z to X. There was no noticeable temperature increase in Y or in the fiberglass inner wall.

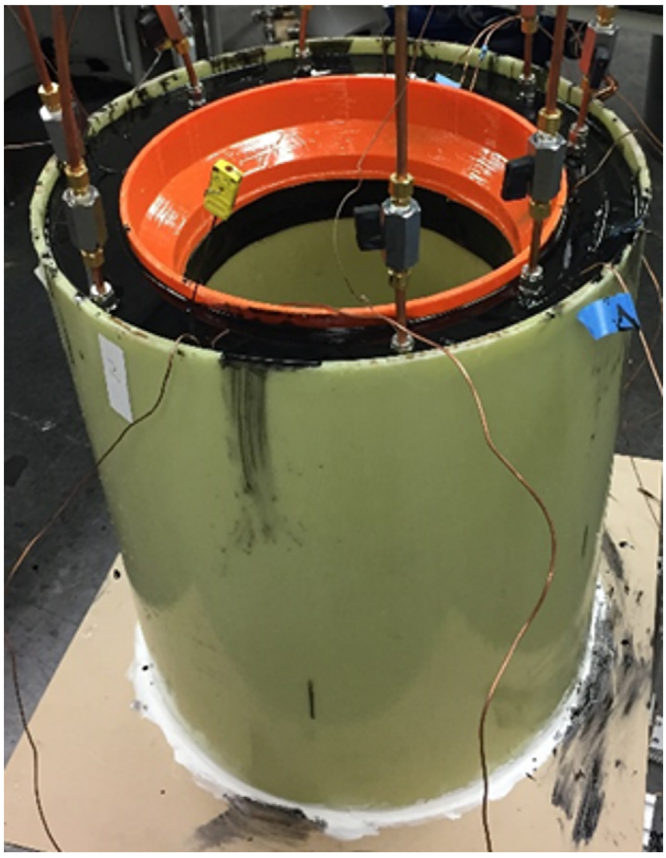

Fig. 4. The prototype three-axis gradient coil. Z gradient was built on a fiberglass cylinder (inner most). X and Y were built on 3D-printed frames (invisible here). They were potted together with epoxy along with a large fiberglass cylinder (outer most). The orange frame is a 3D print of an additional slanted surface parallel to that of the X gradient for epoxy potting.

4. Discussion

There has been a consistent drive for higher magnetic field strength to achieve higher signal to noise ratio and stronger magnetic susceptibility effects, from which neuroimaging (e.g. BOLD fMRI, diffusion MRI) benefits the most. Indeed, 7 T scanners have been approved by FDA for clinical use, and 9.4 T and above are on the horizon [29]. Technically, optimal gradient performance is a pre-requisite to realize the full potential of ultrahigh field MRI. Compared with gradient coils tailored for brain imaging, whole body gradient coils have intrinsically lower gradient efficiency, higher inductance and higher probability of PNS, all of which are critical limiting factors for fast imaging and for high-b factor diffusion imaging. The methods reported here provide solutions to two major limiting factors in current local gradient technologies, namely “shoulder clearance” and heat dissipation.

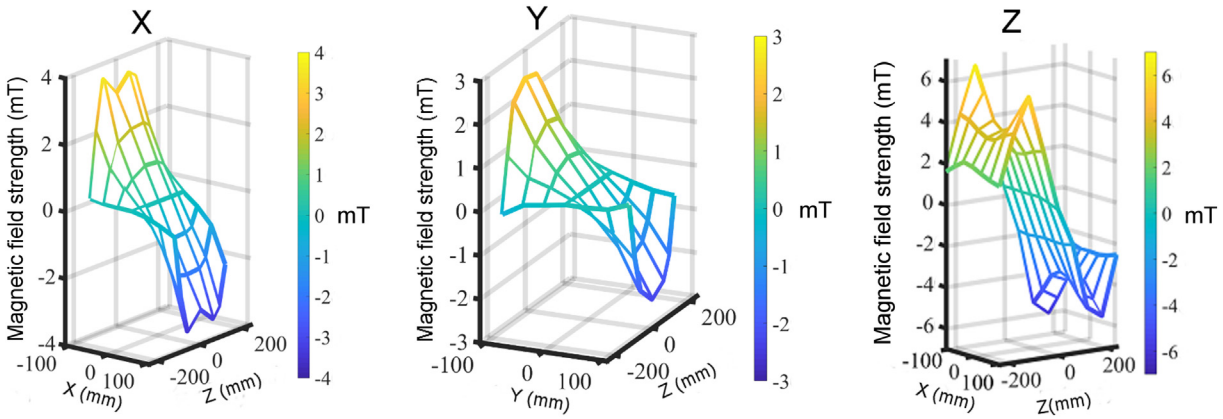

Fig. 5. Field mapping of X, Y and Z gradient coils.

Table 2
Experimental cooling result of the X gradient coil with outer-wall direct cooling.

Sensor temperature (°C)	Time (min)				
	0	3	5	10	15
Inlet	16.5	16.7	16.7	16.6	16.6
Outlet	16.7	17.9	17.9	18.0	18.0
Sensor (XZ1)[a]	25.3	26.6	26.7	26.9	27.1
Sensor (XZ2)[a]	23.9	23.6	23.6	23.7	23.7
Sensor (XY)[a]	25.2	25.3	25.3	25.3	25.3

[a] Sensor XZ1, XZ2 and XY are thermocouple sensors placed between X/Z and X/Y gradients. Measurements were performed using a constant voltage DC power supply, DC current = 42.1 A (100% duty cycle), coolant flow rate = 20.14 LPM; coolant pressure = 98 Pa.

Table 3
Experimental cooling result of the Z gradient coil without outer-wall direct cooling.

Sensor temperature (°C)	Time (min)				
	0	0.5	1	3	6
Inlet	24.5	26.0	27.2	30.3	32.0
Outlet	24.6	26.2	27.3	30.5	32.6
Sensor (XZ)[a]	24.5	27.2	29.3	35.0	45.3
Sensor (ZI)[a]	24.2	24.2	24.3	24.3	24.3
Sensor (XY)[a]	24.4	24.4	24.5	24.6	24.6

[a] Sensor XY, XZ and ZI are thermocouple sensors placed between X/Y and X/Z gradients and between Z and fiberglass of the inner wall. Measurements were performed using a constant voltage DC power supply, DC current = 80 A (100% duty cycle), coolant flow rate = 20.14 LPM. Outer-wall direct cooling was not implemented in Z coil. It was cooled through natural convection by flowing coolant in the neighboring X gradient. Compared with data shown in Table 2, outer-wall direct cooling enhances cooling efficiency.

4.1. Torque, force and acoustic noise

Our gradient coil has a symmetric geometry and should be ideally placed in the center of the magnet. Assuming B_0 is uniform across the coil geometry, it is straightforward to prove that both the net torque and net force that the coil experiences are zero. In a realistic arena, B_0 is not uniform, but is typically symmetric relative to the center of the magnet; it can be proved that the net torque is still zero. But the coil experiences a nonzero net force which can be calculated based on equation $F = \int I \cdot \boldsymbol{dl} \times \boldsymbol{B}(x,y,z)$. Modern magnets have a B_0 uniformity of tens of ppm within a 50 cm sphere, and the variation in B_0 across each wire loop is unlikely to be beyond 2% of B_0. As such, the net force should not be a problem for gradient insert with a symmetric geometry. This is different from asymmetric design, where each wire loop can experience quite different B_0, and thus the torque and force need to be balanced specifically.

While the net force is not of a major concern in symmetric gradient design, the local force and local torque that individual wire segments experience generates acoustic noise [30]. Placing wire segments on the slanted surface as shown in Fig. 1C could potentially exacerbate acoustic noise. Furthermore, the joint between the cylindrical surface and the flaring surface could exacerbate conductor fatigue-related coil failures. These issues warrant further investigation.

4.2. "Flared-end" gradient coil tailored for a head-only MRI system

Limited shoulder clearance has been somewhat unfortunate in conventional head-only gradient coils, as illustrated in Fig. 1A. We take an ergonomic approach, and place the return paths on the slanted planes which lie parallel to the outline of the shoulders. This effectively eliminates the limiting factor from the return paths that contribute to the length of the coil.

Building a coil with an unconventional geometry like this could be challenging. Additive 3D printing technology offers novel opportunities to construct coils with unconventional geometry. Many 3D printing materials are weak in nature and certainly cannot stand the mechanical stress that the wire segments experience in MRI. However, certain 3D printing materials, when immersed in low viscosity epoxy, lead to fiberglass like structures that can be applied to fixate wires in place. Furthermore, new 3D printing materials, such as ceramics, which has very high thermal conductivity and low electrical conductivity, offer novel opportunities for developing next generation technologies to construct coil and to dissipate heat.

In this proof of concept demonstration, we limited the outer diameter of the coil to 46.5 cm—this in turn limited the inner diameter of the coil to only 30 cm. These two parameters combined limited the length of the slanted surface to only 9 cm. As such, only a few return current loops could be placed on the slanted planes. Some return current segments still had to be placed on the cylindrical surface, contributing to the overall length of this coil. Thus, the benefits of flared-end design are fundamentally limited by available flaring surface. There is a tradeoff among available outer diameter, inner diameter and flaring surface.

If one applies the same approach to design a head-only MRI system, i.e. there is no body gradient coil, and assumes the outer diameter to be 70 cm—the inner diameter of many commercial MRI magnets, the inner diameter of the gradient can be much enlarged (e.g. 45 cm), allowing for coil arrays necessary for parallel imaging [5]. The slanted surface can be extended to 14 cm or more, allowing for more return current loops to be placed on this plane, and thus further shortening the overall length of the coil. Furthermore, the enlarged inner diameter and further

away of the return paths from the coil center would warrant a larger ROI with high gradient field fidelity than what have been achieved (Table 1). Additionally, the larger diameter would provide more space for the design of active shielding of eddy current as well. One might anticipate that brain imaging is likely the major application of ultrahigh field MRI scanners (9.4 T or above), the design strategy outlined here can be applied to design next-generation gradient coils tailored for head-only MRI system.

4.3. "Outer-wall direct cooling" vs. "internal-wall direct cooling"

"Internal-wall direct cooling" has been widely used in industry. Nevertheless, this method has several major limitations: i.e. the dilemma between cooling efficiency vs. gradient efficiency. A large size of tube is needed to increase heat conducting areas and reduce pressure drop (enough flow rate), which are necessary to achieve efficient cooling. However, a large tube would lead to low electric current density, hence lowers gradient efficiency. The method presented in this article kills two birds with one stone. It fundamentally resolves this dilemma associated with existing gradient cooling methods. Notably, although our "Outer-wall direct cooling" method was demonstrated in a gradient coil prototype tailored for brain imaging, it can be readily applied to whole body gradient coils as well.

4.4. Coil design method

For coil geometries that warrant analytic solutions, the "target field" approach by Turner [31] is perhaps the most elegant method to derive the optimal current distribution. Our coil has a geometry of "flaired-end", we employed a nonlinear numerical optimization approach to derive the current distribution [9,27]. Our method is efficient in designing Z coil, but it takes long computational times to optimize the X/Y gradient coils. Other methods, such as the boundary element method and stream function method [32–35] may be more efficient in deriving the optimal current distribution for X/Y gradients.

5. Limitations

Active shielding is necessary for advanced imaging applications. In this proof-of-concept study, our purpose was to demonstrate the feasibility to design and construct a coil with an "flared-end" geometry and the outer-wall direct cooling method, we did not implement active shielding due to the complexity in construction. Adding active shielding is possible, and we have performed theoretical optimization (data not shown).

Another limitation is that, we were not able to test this coil inside an MRI scanner due to concerns on scanner warranties. As such, we are not able to demonstrate structural and electrical integrity of the coil fabrication. Our current work is limited to the stage of theoretical feasibility. Nevertheless, the data shown in Table 2 vs. in Table 3 clearly demonstrate the high cooling efficiency achieved with outer-wall direct cooling; Table 1 and Fig. 5 demonstrate the potential of "flared-end" coil geometry in terms of shoulder clearance, gradient field strength and field fidelity volume.

In summary, insufficient shoulder clearance and insufficient cooling are two major technical issues associated with head-only gradient coils. We have presented i) "flared-end" coil design to shorten the overall length of the coil, and ii) "outer wall direct cooling" to dramatically enhance cooling efficiency without compromising gradient efficiency. As a proof of concept, we have built a prototype gradient coil to demonstrate the feasibility. We anticipate that the strategies outline here can be applied to design gradient coils tailored for brain imaging, which is likely the major application of ultrahigh field MRI.

Declaration of Competing Interest

A US patent has been jointly filed by University of Maryland and NIH with regard to the art of this work.

Acknowledgement

This work was partially supported by NIDA Intramural Research Program, NIH (Dr. H. Lu), and by NSF (CBET1336778, Dr. B. Yang).

Appendix A

When coolant flows inside the copper tubing, Ohmic heat generated inside copper tubing will be dissipated to temperature-controlled coolant. The amount of heat removal capability of forced convection inside copper tubing is determined by Newton's Cooling Law [36]:

$$Q = hA\Delta T \tag{A-1}$$

where, Q is the total cooling capacity, A is total heat transfer area between hot source and coolant, h is forced convective heat transfer coefficient, ΔT is the temperature difference between surface and coolant. Higher convective heat transfer coefficient indicates better heat removal capacity of coolant (i.e., better thermal management performance).

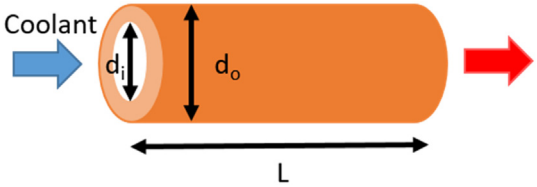

Fig. A1. Schematic of dielectric coolant flowing inside a copper tube.

The nature of coolant internal flow is determined by the Reynolds number. Based on Reynolds number, flow can be either laminar flow or turbulent flow [37].

$$Re = \frac{\rho U d_i}{\mu} \tag{A-2}$$

where ρ is coolant density, U is the coolant velocity, d_i is effective hydraulic diameter, μ is the viscosity.

For ohmic heating generation, heat generated inside the copper tube is uniformly distributed, thus entire copper tube can be treated as uniform heat flux boundary condition. Therefore, the following constant heat flux boundary condition correlations are applicable [38].

$$Nu_{lam} = 4.36 \tag{A-3}$$

$$Nu_{turb} = \frac{\left(f/8\right)(Re-1000)\,Pr}{1 + 12.7\left(f/8\right)^{0.5}\left(Pr^{2/3} - 1\right)} \tag{A-4}$$

$$h = \frac{Nu \bullet k}{d_i} \tag{A-5}$$

where, Nu is Nusselt number (dimensionless), f is friction factor, Pr is Prandtl number, which is material property of coolant, h is convective heat transfer coefficient, k is thermal conductivity of coolant, d_i is effective hydraulic diameter of copper tubing.

$$T_o = T_i + \frac{q_s'' \pi d_i L}{\dot{m} c_p} \tag{A-6}$$

$$T_s = T_o + \frac{q_s''}{h} \tag{A-7}$$

$$q_s'' = \frac{I^2 R_{elec}}{\pi d_o L} \tag{A-8}$$

where, T_o is the coolant outlet temperature, T_i is coolant inlet temperature, q_s'' is the heat flux boundary condition caused by joule heating, I is the current flowing through copper tubing, R_{elec} is the electrical resistance of solid copper wire. d_i is the hydraulic diameter of copper tubing, L is tube total length, $\dot{m}$ is mass flow rate, c_p is the heat capacity of the coolant.

The pressure drop of the coolant at various flow rate through copper tubing is also an important factor to be taken into consideration [38].

$$\Delta P = \frac{\frac{1}{2} f \rho U^2 \frac{L}{d_i}}{1000} \tag{A-9}$$

$$\dot{m} = \frac{1}{4}\pi d_i^2 U \tag{A-10}$$

where f is friction factor, L is the total length, ρ is coolant density. The pressure unit is converted to kPa. $\dot{m}$ is the flow rate inside the copper tubing.

References

[1] Basser PJ, Mattiello J, LeBihan D. MR diffusion tensor spectroscopy and imaging. Biophys J 1994;66(1):259–67.
[2] Chronik B, Rutt B. Constrained length minimum inductance gradient coil design. Magn Reson Med 1998;39(2):270–8.
[3] Turner R. Gradient coil design - a review of methods. Magn Reson Imaging 1993;11(7):903–20.
[4] Setsompop K, Kimmlingen R, Eberlein E, Witzel T, Cohen-Adad J, McNab J, et al. Pushing the limits of in vivo diffusion MRI for the human connectome project. Neuroimage 2013;80:220–33.
[5] Lee SK, Mathieu JB, Graziani D, Piel J, Budesheim E, Fiveland E, et al. Peripheral nerve stimulation characteristics of an asymmetric head-only gradient coil compatible with a high-channel-count receiver array. Magn Reson Med 2016;76(6):1939–50.
[6] Zhang B, Yen Y, Chronik B, McKinnon G, Schaefer D, Rutt B. Peripheral nerve stimulation properties of head and body gradient coils of various sizes. Magn Reson Med 2003;50(1):50–8.
[7] Turner R, Le Bihan D, Maier J, Vavrek R, Hedges LK, Pekar J. Echo-planar imaging of intravoxel incoherent motion. Radiology 1990;177(2):407–14.
[8] Turner R, Le Bihan D, Chesnick AS. Echo-planar imaging of diffusion and perfusion. Magn Reson Med 1991;19(2):247–53.
[9] Wong EC, Jesmanowicz A, Hyde JS. Coil optimization for MRI by conjugate gradient descent. Magn Reson Med 1991;21(1):39–48.
[10] Wong EC, Jesmanowicz A, Hyde JS. High-resolution, short echo time MR imaging of the fingers and wrist with a local gradient coil. Radiology 1991;181(2):393–7.
[11] Turner R, Le Bihan D, Moonen CT, Despres D, Frank J. Echo-planar time course MRI of cat brain oxygenation changes. Magn Reson Med 1991;22(1):159–66.
[12] Bandettini PA, Wong EC, Hinks RS, Tikofsky RS, Hyde JS. Time course EPI of human brain function during task activation. Magn Reson Med 1992;25(2):390–7.
[13] Wade TP, Alejski A, Tsarapkina Janos, Rutt Dina, Brian K, CA McKenzie. Thermal characterization of an all hollow copper insertable head gradient coil. Proc Int Soc Magn Reson Med 2015:1021.
[14] Tomasi D, Xavier RF, Foerster B, Panepucci H, Tannús A, Vidoto EL. Asymmetrical gradient coil for head imaging. Magn Reson Med 2002;48(4):707–14.
[15] Abduljalil AM, Aletras AH, Robitaille PM. Torque free asymmetric gradient coils for echo planar imaging. Magn Reson Med 1994;31(4):450–3.
[16] Alsop D, Connick T. Optimization of torque-balanced asymmetric head gradient coils. Magn Reson Med 1996;35(6):875–86.
[17] Crozier S, Doddrell D. A simple design methodology for elliptical cross-section, transverse, asymmetric, head gradient coils for MRI. IEEE Trans Biomed Eng 1998;45(7):945–8.
[18] vom Endt A, Kimmlingen R, Riegler J, Eberlein E, Schmitt F. A high-performance head gradient coil for 7T systems. Proc Int Soc Magn Reson Med 2006:1370.
[19] Mathieu J-B, Lee S-KG, Lin Dominic, Budesheim Jian, Piel Eric, Joseph E, et al. Development of a dedicated asymmetric head-only gradient coil for high-performance brain imaging with a high PNS threshold. Proc Int Soc Magn Reson Med 2015:1019.
[20] Meier C, Zwanger M, Feiweier T, Porter D. Concomitant field terms for asymmetric gradient coils: consequences for diffusion, flow, and echo-planar imaging. Magn Reson Med 2008;60(1):128–34.
[21] Tan E, Lee S, Weavers P, Graziani D, Piel J, Shu Y, et al. High slew-rate head-only gradient for improving distortion in echo planar imaging: preliminary experience. J Magn Reson Imaging 2016;44(3):653–64.
[22] Tao S, Trzasko J, Gunter J, Weavers P, Shu Y, Huston J, et al. Gradient nonlinearity calibration and correction for a compact, asymmetric magnetic resonance imaging gradient system. Phys Med Biol 2017;62(2):N18–31.
[23] Wade TP, Alejski AB, Tsarapkina Janos, Hinks Dina, Scott McKinnon R, Graeme C, et al. Design, construction and initial evaluation of a folded insertable head gradient coil. Proc Int Soc Magn Reson Med 2014:4851.
[24] Amm BC, Aksel B, Wangerin KA. Transversely folded gradient coil USA 2011.
[25] Bowtell R, Peters A. Analytic approach to the design of transverse gradient coils with co-axial return paths. Magn Reson Med 1999;41(3):600–8.
[26] Mansfield P, Chapman B, Bowtell R, Glover P, Coxon R, Harvey P. Active acoustic screening - reduction of noise in gradient coils by Lorentz force balancing. Magn Reson Med 1995;33(2):276–81.
[27] Lu H, Jesmanowicz A, Li SJ, Hyde JS. Momentum-weighted conjugate gradient descent algorithm for gradient coil optimization. Magn Reson Med 2004;51(1):158–64.
[28] Wong EC, Jesmanowicz A, Hyde JS. Echo-planar imaging of the human brain using a three axis local gradient coil. 1992. p. 105. Berlin.
[29] Vaughan T, DelaBarre L, Snyder C, Tian J, Akgun C, Shrivastava D, et al. 9.4T human MRI: preliminary results. Magn Reson Med 2006;56(6):1274–82.
[30] Doty FD, Blumler P, Blumich B, Botto R, Fukushima E. MRI gradient coil optimization. Spatially resolved magnetic resonance. vol. 1. Germany: WILEY-VCH Verlag GmbH; 1998. p. 647–74.
[31] Turner R. A target field approach to optimal coil design. J Phys D Appl Phys 1986;19(8):L147–51.
[32] Pissanetzky S. Minimum energy MRI gradient coils of general geometry. Meas Sci Technol 1992;3(7):667–73.
[33] Lemdiasov RA, Ludwig R. A stream function method for gradient coil design. Concepts Magn Reson Part B: Magn Reson Eng 2005;26B(1):67–80.
[34] Poole M, Bowtell R. Novel gradient coils designed using a boundary element method. Concepts Magn Reson Part B: Magn Reson Eng 2007;31B(3):162–75.
[35] Handler W, Harris C, Scholl T, Parker D, Goodrich K, Dalrymple B, et al. New head gradient coil design and construction techniques. J Magn Reson Imaging 2014;39(5):1088–95.
[36] Patankar SV. Computation of conduction and duct flow heat transfer. New York: Routledge; 1991.
[37] Piasecka M. Impact of selected parameters on refrigerant flow boiling heat transfer and pressure drop in minichannels. Int J Refrig 2015;56:198–212.
[38] Bergman TL, Incropera FP, DeWitt DP, Lavine AS. Fundamentals of heat and mass transfer. John Wiley & Sons; 2011.